

# SIMULATION OF COMPLEX 3D BEHAVIOR OF MASONRY ARCH SYSTEMS

by

Bora Pulatsu

A DISSERTATION

Presented to the Faculty of  
The Graduate College at the University of Nebraska  
In Partial Fulfilment of Requirements  
For the Degree of Doctor of Philosophy

Major: Architectural Engineering

Under the Supervision of Professor Ece Erdogmus

Lincoln, Nebraska

May, 2019

ProQuest Number: 13902180

All rights reserved

INFORMATION TO ALL USERS

The quality of this reproduction is dependent upon the quality of the copy submitted.

In the unlikely event that the author did not send a complete manuscript and there are missing pages, these will be noted. Also, if material had to be removed, a note will indicate the deletion.



ProQuest 13902180

Published by ProQuest LLC (2019). Copyright of the Dissertation is held by the Author.

All rights reserved.

This work is protected against unauthorized copying under Title 17, United States Code  
Microform Edition © ProQuest LLC.

ProQuest LLC.  
789 East Eisenhower Parkway  
P.O. Box 1346  
Ann Arbor, MI 48106 – 1346

# SIMULATION OF COMPLEX 3D BEHAVIOR OF MASONRY ARCH SYSTEMS

Bora Pulatsu, Ph.D.

University of Nebraska, 2019

Advisor: Ece Erdogmus

Masonry structures constitute a large portion of architectural heritage all around the world in the form of post-lintel systems; walls, arches, vaults and domes in buildings and masonry arch bridges. Since it is such a dominant construction material, achieving realistic numerical models of complex masonry structures is of particular interest to better understand their structural behavior and avoid unnecessary or poor interventions.

This dissertation makes several contributions to the state of the art of modeling complex masonry arch systems.

First, in discontinuum analysis commonly used contact models in tension (tension cut-off) does not capture the complete response of the material and also does not include mode-I fracture energy which leads to the underestimation of the capacity. In this context, present dissertation proposes new contact models to be incorporated into the discrete element method (DEM) to more accurately simulate the tensile softening in quasi-brittle materials, such as masonry, with an emphasis on fracture mechanism and post-peak response. As an important novel contribution, the proposed computational models successfully represent the complete (pre- and post- peak) material behavior and realistically replicate the cracking mechanism.

Second, the discontinuum modeling strategy is extended to analyze the masonry arches and it is compared with different modeling strategies, namely limit state and sequential linear analysis. All numerical models are validated via experimental results and sensitivity analyses are performed on the mechanical properties of the material.

Third, a novel 3D representation of masonry arch bridges is achieved using mixed discrete-continuum approach and it is validated with several experimental studies. With this modeling strategy, two main contributions are achieved; first, triggering mechanisms for the out of plane failure of spandrel walls are established; second, the influence of soil backfill on the behavior and strength of the bridges is better understood through a comprehensive parametric study. Transverse effects, damage patterns and collapse mechanisms are discussed under different types of loading considering different arch bridge models, representing common geometrical properties in the northwest Iberian Peninsula. The analysis demonstrates the severe capacity reduction due to spandrel wall failures and the importance of soil backfill in the behavior of these systems. These observations were, only possible by utilizing the proposed mixed numerical modeling strategy. Hence, a better understanding of masonry arch bridge behavior is accomplished by taking into account the soil-structure interaction problem.

PREVIEW

To my wife

## ACKNOWLEDGEMENT

I would like to express my gratitude to Professor Erdogmus for her immense support and encouragement throughout my research. I cannot thank her enough for the opportunities she provided me during my PhD journey and her profound belief in my work. I would like to declare my special appreciation and gratefulness to Professor Lourenço who has significant touches in every part of my dissertation. I need to emphasize his unwavering support and guidance since my masters.

I am particularly grateful to Dr. Eduardo Bretas, not only for his great friendship but also his valuable contributions and fruitful discussions. I deeply appreciate his guidance. In addition, I wish to acknowledge Dr. Romain Quey for his contributions, which I believe it makes an important impact on the discontinuum analysis of quasi-brittle materials. I would like to extend my thanks to Professor Jay Puckett for his valuable discussions and providing me the technical support to pursue my studies efficiently. A special thanks to Dr. Jim Hazzard and Dr. Jose V. Lemos for their mentorship and technical support in discrete element modeling. Also, I would like to express my gratitude to Itasca Educational Partnership Program (IEP) for their kind support and providing 3DEC software. I am deeply indebted to Dr. Engin Karaesmen and Dr. Erhan Karaesmen, for their endless support and guidance. It is also my pleasure to meet with Professor Kagan Tuncay, who inspired me to focus on computational modeling.

This journey would not have been possible and more meaningful without endless love and untiring support of my wife, Ezgi Pulatsu. I cannot begin to express my thanks to my mother; Serap Pulatsu and my father; Şafak Pulatsu, having a precious place in my

heart that words are not enough to describe my feelings. Finally, I take this opportunity to thank my dear friends who were always there when I needed them the most from all around the world.

PREVIEW

## TABLE OF CONTENTS

CHAPTER 1.	Introduction .....	1
1.1	Background and Motivation.....	2
1.2	Goals and Objectives.....	5
1.3	Scope .....	6
1.4	Dissertation Overview.....	7
1.5	Contributions/Significance.....	8
CHAPTER 2.	Literature Review on Masonry Assemblages and Arched Structures ..	11
2.1	Masonry.....	11
2.2	Mechanics of Masonry Assemblages .....	12
2.2.1	Uniaxial Compression Test of Masonry .....	14
2.2.2	Uniaxial Tension Tests of Masonry.....	16
2.2.3	Shear Test of Masonry .....	18
2.2.4	Biaxial Loading.....	19
2.3	Numerical Investigations on Masonry Arch Systems .....	21
2.3.1	Early Motivations.....	22
2.3.2	Classic Theories.....	23
2.3.3	Limit (Plastic) Analysis .....	24
2.3.4	Advanced Numerical Solution to Analyze Masonry Arch Structures .....	27
CHAPTER 3.	Investigations on the Softening Behavior of Quasi-Brittle Materials via Discontinuum Analysis .....	41
3.1	Introduction .....	41
3.2	Benchmark Studies from Literature .....	44
3.2.1	Direct Tension Test of Concrete .....	44
3.2.2	Direct Tension Test of Stack Bonded Masonry Prism.....	45
3.3	Discrete Modeling Strategy.....	46
3.4	Contact Constitutive Laws in Tension .....	51
3.5	Geometrical Representation of Concrete and Masonry Specimen.....	53
3.5.1	Simplified Meso-Model (SMM).....	53
3.5.2	Detailed Meso-Model (DMM).....	54



3.6	Discontinuum Analysis of the Tensile Behavior of the Concrete Specimen .....	56
3.6.1	Macro- and Micro- Material Properties .....	57
3.6.2	Results of Simplified and Detailed Meso-Models .....	58
3.7	Sensitivity Analysis on the Contact Parameters using DMM .....	61
3.7.1	Prediction of the Fracture Mechanism .....	65
3.8	Discontinuum Analysis of the Tensile Behavior of Masonry Prism.....	69
3.8.1	Material and Contact Properties.....	70
3.8.2	Prediction of Failure Model for Masonry Assemblages under Direct Tension	71
3.9	Summary and Discussion .....	75
CHAPTER 4.	Simulation of Masonry Arch Mechanics.....	78
4.1	Linear Programming .....	79
4.2	Discrete Element Modeling.....	87
4.2.1	Discrete Element Validation for Masonry Arches.....	88
4.2.2	In-Plane Mechanism: DEM vs LSA .....	92
4.2.3	In-Plane Mechanism: DEM vs Small-Scale Experiment (Tilting Test) .....	96
4.2.4	3D Failure Modes of Masonry Arches.....	102
4.3	Continuum Analysis: SLA .....	110
4.3.1	Mathematical Background.....	111
4.3.2	Finite Element Approximation .....	114
4.3.3	Sequentially Linear Analysis .....	118
4.3.4	Proportional Loading: Applications on Masonry Arches .....	124
4.3.5	Non-proportional loading: Application on Masonry Arch .....	127
4.4	Comparison of SLA and DEM: Discrete crack model vs Smear crack model	132
4.5	Summary and Discussion .....	141
CHAPTER 5.	Analysis of the Complex 2D and 3D Behavior of Arch Bridges .....	143
5.1	2D Discrete Element Modeling of Masonry Arch Bridges.....	145
5.2	Parametric Analysis using the Validated 2D Discrete Element Modeling Strategy .....	150

5.2.1	Geometry of the Base Model .....	150
5.2.2	Effect of the Backfill and Spandrel Wall .....	151
5.2.3	Effect of Boundary Conditions on the Load Carrying Capacity .....	154
5.2.4	Effect of the Morphology of the Arch Barrel (Number of Layers and Bond Pattern) .....	157
5.3	Investigations on the Skew Masonry Arches .....	161
5.4	3D Mixed Discrete-Continuum (MDC) Approach .....	167
5.4.1	Soil Model Validation .....	172
5.4.2	Validation of the Mixed Discrete-Continuum Approach .....	174
5.4.3	Representative Masonry Arch Bridge Models .....	189
5.4.4	2D and 3D Modeling of Masonry Arch Bridges .....	193
5.4.5	Parametric Study on Backfill Properties using LSA and DEM .....	196
5.4.6	Discussion on Spandrel Wall Behavior .....	197
5.4.7	Stiff and Soft Soil Backfill Effect on the Behavior of Spandrel Walls ....	203
5.4.8	In-Plane (IP) and Out-of-Plane (OOP) Capacity Difference of Masonry Arch Bridge .....	207
5.5	Summary and Discussion .....	212
CHAPTER 6.	Conclusions .....	215
CHAPTER 7.	Bibliography .....	221

## LIST OF FIGURES

Figure 1-1. Masonry arch bridge terminology (Gilbert 2016).....	2
Figure 2-1. Different kinds of stone walls .....	13
Figure 2-2. Fracture pattern of stack bonded masonry prism under uniaxial compression test (soft mud brick), taken from (Vermeltfoort 2005).....	14
Figure 2-3. Uniaxial compression test of masonry panel with different orientation of bed joints (Page 1981). .....	15
Figure 2-4. Post-peak behavior of bond under direct tension (Shaded area indicated the envelope of the test experimental results), (Lourenço 1996).....	17
Figure 2-5. Uniaxial tension test of brickwork masonry panel with different bed-joint orientation (Dhanasekar et al. 1985). .....	18
Figure 2-6. Different test configuration for shear testing (Lourenço and Ramos 2004) ..	18
Figure 2-7. Biaxial strength of masonry panels (Page 1981, 1982).....	21
Figure 2-8. Limit Analysis of arch structures obtained via LP (Livesley 1992) .....	26
Figure 2-9. Modeling strategies for masonry structures (Lourenço 2002) .....	28
Figure 2-10. Masonry arch bridge analysis via frame element (Boothby 2001). .....	29
Figure 2-11. Iterative algorithm to assess masonry arch bridges a) $(k-1)^{th}$ iteration; b) prediction; and c) correction (Brencich and De Francesco 2004a).....	31
Figure 2-12. In-plane analysis of an arch system (Loo and Yan 1991). .....	32
Figure 2-13. 3D Finite element model, Vilanova Bridge (Conde et al. 2017). .....	34
Figure 2-14. Seismic behavior of the stand-alone masonry arches (Lemos 1998).....	36
Figure 2-15. 3D model of Pont Julien, consisting of 1219 rigid blocks (Rafiee and Vinches 2013). .....	39
Figure 3-1. (a) Illustration of direct tension test of a concrete specimen (dimensions are in mm) (b) Stress-displacement curve obtained from the displacement-controlled experiment (Hordijk 1991). .....	45
Figure 3-2. Test setup and results obtained from uniaxial tensile test.....	46
Figure 3-3. Representation of contact point between rectangular blocks with triangular finite-difference zones (2D). .....	49
Figure 3-4. Dynamic calculation cycle performed in 3DEC. ....	50
Figure 3-5. Contact constitutive models in tension; initial contact normal stiffness (kn).51	

Figure 3-6. Coulomb-slip joint model; initial contact shear stiffness ( $k_s$ ), cohesion ( $c$ ) and friction angle ( $\phi$ ).....	52
Figure 3-7. Simplified model of concrete and masonry prisms, consisting of two separate blocks with a smooth contact surface. ....	54
Figure 3-8. Representation of concrete and masonry prism specimens using a tessellation into polyhedral blocks.....	55
Figure 3-9. Representation of the detailed meso model: joined polyhedral blocks at the bottom and top and discrete polyhedral blocks in between. ....	57
Figure 3-10. Different tensile contact models compared with the experimental result (TC for tension cut-off, LS for linear softening and PS for polynomial softening).....	60
Figure 3-11. Comparison of experimental and numerical results (polynomial softening is shown).....	61
Figure 3-12. Influence of cohesion ( $c$ ) on the stress-displacement response of the discrete element model.....	62
Figure 3-13. Influence of fracture energy ( $G_f$ ) on the stress-displacement response of the discrete element model. ....	63
Figure 3-14. Influence of the grain number (GN) on the macro behavior for different fracture energies.....	64
Figure 3-15. Influence of the dilation ( $\psi$ ) on the stress-displacement response of discrete element model.....	65
Figure 3-16. Influence of boundary conditions on the cracking mechanism and stress-material behavior.....	66
Figure 3-17. Failure mechanism of a notched concrete specimen under direct tension (rotatable boundary condition).....	67
Figure 3-18. Failure mechanism of a notched concrete specimen under direct tension (fixed boundary condition).....	68
Figure 3-19. Failure modes of stack bonded masonry prisms under uniaxial tension test. ....	70
Figure 3-20. Macro behavior of the model for different elastic modulus of the masonry constituents. ....	72

Figure 3-21. Influence of weak and strong mortar on the macro behavior of masonry prism specimens; $(f_t)_{\text{interface}} = 0.4 \text{ MPa}$ , $(G_f)_{\text{interface}} = 10 \text{ N/m}$ .....	73
Figure 3-22. Detailed meso-model; Continuum Blocks (Masonry Units) and Discrete Polyhedral Blocks (Mortar). ....	73
Figure 3-23. Parametric analysis on the detailed meso model ( $(f_t)_{\text{mortar}} = (f_t)_{\text{interface}}$ ). ....	74
Figure 3-24. Partial failure of mortar obtained via detailed meso model. ....	75
Figure 4-1. General workflow performed in this chapter. ....	78
Figure 4-2. Equilibrium state of a voussoir. ....	82
Figure 4-3. Medium span masonry arches. ....	84
Figure 4-4. LSA of deep medium span masonry arch. ....	85
Figure 4-5. LSA of shallow medium span masonry arch. ....	86
Figure 4-6. Masonry arches; $r/s: 0.5$ and $r/s: 0.23$ , discrete element models.....	89
Figure 4-7. Parametric study on number of blocks and contact stiffness compared with analytical solutions.....	91
Figure 4-8. Representation of the loading positions (LP) on a medium span deep arch. .	93
Figure 4-9. Capacity curve of shallow medium span arch.....	93
Figure 4-10. Collapse mechanism of deep arch; DEM and LSA. ....	94
Figure 4-11. Representation of the loading positions (LP) on a medium span shallow arch. ....	95
Figure 4-12. Ultimate load vs span for a shallow medium span arch.....	95
Figure 4-13. Collapse mechanism of shallow arch; DEM and LSA ....	96
Figure 4-14. Discrete Element Models; Left: Circular Arch, Right: Point Arch.....	97
Figure 4-15. Representation of tilting test. ....	98
Figure 4-16. Imminent plastic hinges and collapse mechanism of a small-scale circular arch.....	100
Figure 4-17. Experimental results of the tilting tests and numerical predictions. ....	101
Figure 4-18. Sensitivity analysis on the contact friction angle of the discrete element model and validation with experimental study. ....	104
Figure 4-19. Points loads applied on shallow and deep medium span arches. ....	105

Figure 4-20. Load vs displacement curves for shallow medium span arch with different contact friction angles (FA) and loading points.....	106
Figure 4-21. Damage patterns of <i>shallow medium span arch</i> under vertical point load for different contact friction angles. ....	107
Figure 4-22. Load vs displacement curves for deep medium span arch with different contact friction angles (FA) and loading points. ....	108
Figure 4-23. Damage patterns of <i>deep medium span arch</i> under vertical point load for different contact friction angles. ....	109
Figure 4-24. Representation of a cantilever elastic beam under dead and traction load.	112
Figure 4-25. Stress-strain curve and saw-tooth approximation. ....	120
Figure 4-26. Loading and boundary conditions of the analyzed beam (dimension is given in mm).....	122
Figure 4-27. Comparison of SLA and experiment.....	122
Figure 4-28. Finite element models generated via unstructured triangular mesh.....	123
Figure 4-29. Sensitivity analysis on the mesh-size.....	124
Figure 4-30. Representation of a) hypothetical masonry arch and b) corresponding finite element model.....	125
Figure 4-31. Failure mechanism obtained via SLA.....	126
Figure 4-32. Sensitivity analysis on the number of element (NEL) and fracture energies. ....	127
Figure 4-33. Analyzed masonry arch under non-proportional loading.....	130
Figure 4-34. Comparison of experimental peak load and continuum analysis.....	131
Figure 4-35. Collapse damage state of arch barrel under non-proportional loading. ....	132
Figure 4-36. Discrete element model prepared for the notched beam analysis. ....	133
Figure 4-37. Comparison of continuum and discontinuum analysis. ....	134
Figure 4-38. Sensitivity analysis on the number of contact point in discrete element models. ....	135
Figure 4-39. Force-displacement curves corresponding to different mesh refinements.	135
Figure 4-40. Comparison of continuum and discontinuum analysis with different fracture energies. ....	136
Figure 4-41. Loading condition and collapse mechanism of a masonry arch subjected to proportional loading.....	137

Figure 4-42. Comparison of discrete and smear crack models with different fracture energies. ....	139
Figure 4-43. Loading condition and collapse mechanism of a masonry arch subjected to non-proportional loading. ....	140
Figure 4-44. Comparison of discrete and smear crack model (non-proportional loading). ....	141
Figure 5-1. General work flow to assess masonry arch bridges .....	145
Figure 5-2. Capacity curves obtained via discrete element model and comparison with limit analysis and experimental peak load.....	148
Figure 5-3. Experiment and discontinuum analysis of true scale brickwork masonry arch bridge. ....	149
Figure 5-4. Dimensions of the base model and the arrangement of rigid blocks in the discontinuum model.....	151
Figure 5-5. Force-displacement curve of arch and arch-backfill systems under vertical point load acting at the quarter span. ....	153
Figure 5-6. Force-displacement curves for different spandrel wall (SW) thicknesses. ...	154
Figure 5-7. Boundary conditions. ....	155
Figure 5-8. Capacity curves and corresponding failure mechanism. ....	157
Figure 5-9. Double-layer (or multi-ring) masonry arch bridge models with different bond patterns.....	158
Figure 5-10. Force vs. displacement curves for different arch barrel morphologies and corresponding collapse mechanism. ....	159
Figure 5-11. Parametric study for tensile strength at the contact located at the arch barrel. ....	161
Figure 5-12. Construction techniques: Helicoidal method (A) and False skew (B). ....	162
Figure 5-13. Damage state – Plan view (Left: Experiment: (Hodgson 1996), Right: Numerical Model). ....	163
Figure 5-14. Damage state – Intrados (Right: Experiment (Hodgson 1996), Left: Numerical model) .....	165
Figure 5-15. Double layer (3m span) skew masonry arch barrel (Experimental and numerical damage states).....	166

Figure 5-16. Applied numerical modeling strategy (mixed discrete-continuum approach) and representation of the interaction between masonry blocks and masonry-soil.....	168
Figure 5-17. Strip footing on elasto-plastic soil.....	173
Figure 5-18. Comparison of the numerical predictions for the strip footing problem....	174
Figure 5-19. 3DEC model – Bolton Institute Bridge.....	175
Figure 5-20. Comparison of experimental and numerical results.....	176
Figure 5-21. Progressive failure mechanism of masonry arch model loaded at the quarter span. ....	178
Figure 5-22. Influence of the elastic modulus of the backfill (boxed values) on the masonry arch bridge response. ....	179
Figure 5-23. Sensitivity analysis of the inelastic contact parameters; cohesion and friction angle.....	180
Figure 5-24. Large-scale bridge model.....	181
Figure 5-25. LVDT configuration and loading condition (Boothby et al. 2005). ....	182
Figure 5-26. Discrete-continuum model (DCM) consisting of side supports, spandrel walls, arch barrel and backfill material. ....	184
Figure 5-27. Discrete continuum models with different boundary conditions. ....	185
Figure 5-28. Force-displacement curves obtained from different boundary conditions. ....	186
Figure 5-29. Shifting of spandrel wall and tensile cracks on the spandrel wall. ....	187
Figure 5-30. Force vs displacement curves for different friction angles (FA) between masonry and soil (M-S). ....	188
Figure 5-31. Representative masonry arch bridge models.....	190
Figure 5-32. DMS under different loading patterns.....	192
Figure 5-33. Collapse mechanism of shallow masonry arch bridge with short span models. ....	195
Figure 5-34. Comparison the results of limit state and discontinuum analysis. ....	196
Figure 5-35. Influence of backfill properties (friction and cohesion) on the 2D limit state analysis and 3D discrete element models, for semi-shallow arch bridge with short span. ....	197
Figure 5-36. Spandrel wall deflection (Point Donim, Portugal).....	198
Figure 5-37. Monitoring points on arch barrel (R1) and spandrel wall (R2).....	199
Figure 5-38. Spandrel wall failure of DMS (Colors display displacement magnitude). ....	200



Figure 5-39. Spandrel wall failure DSS (Colors display displacement magnitude). .....	201
Figure 5-40. Out-of-plane displacement and the longitudinal cracks at the intrados of the arch barrel (Colors display displacement magnitude). .....	201
Figure 5-41. Capacity curves of four representative bridge model under two types of loading.....	202
Figure 5-42. In-plane collapse mechanism of DMS under knife edge loading (Colors display displacement magnitude).....	203
Figure 5-43. Discrete element model of Donim Bridge. ....	205
Figure 5-44. Structural behavior of Donim Bridge (structural and non-structural backfill). .....	206
Figure 5-45. Mixed discrete-continuum models with inclined boundary conditions. ....	208
Figure 5-46. A typical in-plane collapse mechanism (RING). .....	209
Figure 5-47. Capacity curves based on the backfill height both in-plane (IP) and out-of-plane (OOP) directions. ....	210
Figure 5-48. Collapse mechanism of arch bridges with respect to slenderness ratio of spandrel walls.....	211
Figure 5-49. Capacity vs slenderness ratio of the spandrel walls, $t/H$ (thickness of the wall/height of the wall at the crown). ....	211
Figure 5-50. Transverse strength of the analyzed bridge geometry considering boundary conditions.....	212

## LIST OF TABLES

Table 3-1. Contact properties used in the two types of model.....	58
Table 3-2. Reference contact and material properties. ....	61
Table 3-3. Contact properties used in the simplified meso model.....	70
Table 3-4. Reference contact properties used in the detailed meso model. ....	71
Table 4-1. Geometrical properties of reference masonry arches. ....	84
Table 4-2. Geometrical properties of the model arch barrel. ....	102
Table 4-3. Material and contact properties .....	103
Table 4-4. Ultimate load obtained via discontinuum analysis for different contact friction angles and corresponding collapse mechanisms.....	104
Table 4-5. Material properties – 4-point bending test of concrete beam. ....	121
Table 4-6. Material Properties used in SLA .....	125
Table 4-7. Material and contact properties. ....	133
Table 4-8. Material and contact properties used in discontinuum analysis (proportional loading). ....	137
Table 4-9. Material and contact properties used in discontinuum analysis (non-proportional loading).....	139
Table 5-1. Geometrical Properties (in meters).....	146
Table 5-2. Material Properties (BA2) .....	146
Table 5-3. Contact Properties. ....	147
Table 5-4. Contact and material properties of the discrete element model. ....	163
Table 5-5. Load carrying capacity of 3-meter span skew arch model constructed with helicoidal and false methods.....	167
Table 5-6. Material properties of the soil.....	173
Table 5-7. Backfill and contact properties (Bolton Institute Bridge) .....	176
Table 5-8. Geometrical properties of model bridge.....	181
Table 5-9. Soil backfill properties. ....	182
Table 5-10. Contact properties in the discrete-continuum model.....	183
Table 5-11. Geometrical properties of the representative masonry arch bridges (dimensions are in meters).....	189
Table 5-12. Reference material and contact properties (M-M: contact parameters between masonry and masonry, M-S: contact parameters between masonry and soil).....	194

Table 5-13. Geometrical .....	204
Table 5-14. Backfill and contact properties (Donim Bridge) .....	205
Table 5-15. Maximum displacement values (mm) for two different soil backfill stiffnesses. .....	207

PREVIEW

## CHAPTER 1 INTRODUCTION

Throughout history, masonry arches were used to span relatively large distances as a common structural form dating back to the Roman Empire. Many of them are still in use in road and railway networks in Europe and the northeastern United States. Until the first half of the nineteenth century, the design and analysis of these structures had been performed by using empirical methods and common construction techniques (Brencich and Morbiducci 2007). With recent developments in modern mechanics and the increased computational capacity, more detailed structural analysis of masonry arches became possible. Notwithstanding that experimental studies of masonry arch systems require material sources and time for the construction of the scaled model of existing structures. This process may be costly and time intensive. Moreover, it may be difficult to replicate the existing conditions of a structure in the laboratory environment, since there are many uncertainties about the material properties, geometrical parameters, and boundary conditions. With the help of the advanced modelling techniques, full-scale representation of existing structures is possible, where various input parameters can be varied to understand the behavior an existing structure under various type of loadings in a time manageable manner.

In this chapter, a brief introductory about the masonry arch bridge components and up-to-date computational modeling strategies are presented. Then, the summary of the dissertation is given together with the contributions and significance of the present study.

## 1.1 Background and Motivation

A masonry arch bridges has a composite and highly heterogeneous structural form where all of the components interact with each other in a complex manner. The commonly used terminology for the components of a masonry arch bridge is given in Figure 1-1.

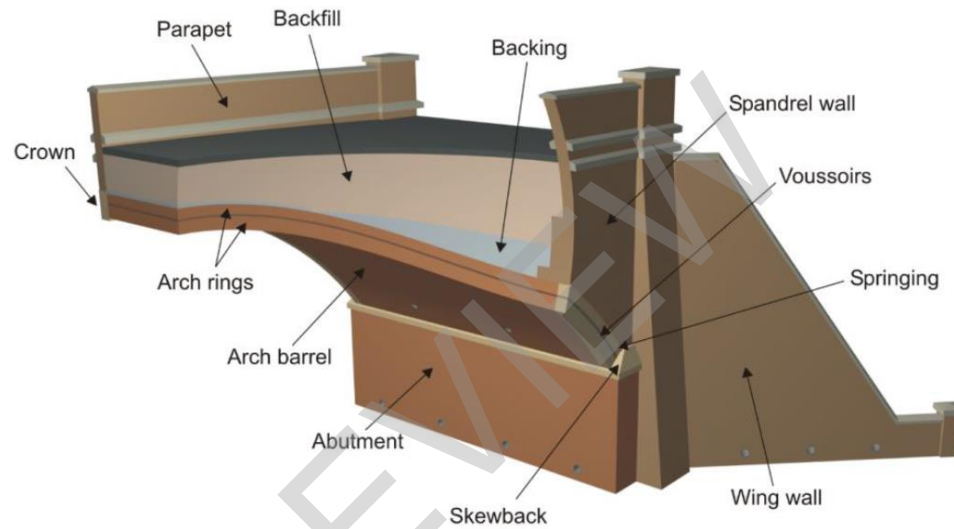


Figure 1-1. Masonry arch bridge terminology (Gilbert 2016).

The main component of a masonry arch bridge is the arch barrel, or barrel vault, which may have varying cross-sections and arch curvatures (shallow, circular and pointed). It may be composed of single or multiple layers of masonry arches constructed with different bond patterns (running bond, stack bond, etc.). Each masonry arch bridge has unique construction details and morphology due to workmanship, local practices and material availability. These unique properties of the structure may yield to noticeable differences on the load carrying capacity and failure mechanism of the structure.

The soil backfill and spandrel walls are the other important load bearing components of a masonry arch bridge. The backing material is typically constructed with earthen materials, i.e. sand, clay or rubble stone. The spandrel walls are constructed of masonry, typically in similar style to the arch barrel, but may also be different. The spandrel wall contains the soil backfill and connects the arch barrel to the approach roads and abutments providing lateral support to the arch. Because of this, spandrel walls work like a retaining wall and are subjected to transversal earth pressures due to soil. In addition, spandrel wall thickness may change through the height of bridges, generally decreasing towards the top. The backfill provides two main advantages. First, it compresses the arch and increases the axial compression inside the arch barrel. This prestressed condition provides higher load carrying capacity. Second, it distributes the live loads on the load bearing arch form, which eliminates possible stress concentrations. Each of these structural elements provide unique characteristics to masonry arch bridges in terms of strength, stiffness and structural behavior. These contributions will be explored through the advanced modeling strategies in this dissertation.

There are different methods to analyze masonry arch systems, which vary depending on the level of accuracy and the knowledge of material properties. Sarhosis et al. (2016) divides current assessment methods into three main categories, *i)* semi-empirical models, *ii)* equilibrium-based models and *iii)* numerical models. The most practical and widely used semi-empirical technique is the MEXE method, developed in 20<sup>th</sup> century for quick assessment of load carrying capacity of masonry arch bridges. However, this approach does not consider the influence of arch geometry and spandrel walls. Furthermore, it overestimates the capacity of short span arch bridges, while it may provide conservative results for spans over 12 meters (Wang et al. 2013). On the other

hand, limit state analysis (LSA) is another practical and fast solution to estimate the failure load of masonry arch bridges. It requires few input parameters and it may provide a simple consideration of the passive and active earth pressures acting on the arch barrel. Although, simplified modeling of soil backfill yields less sophisticated numerical models, it may be under estimating the load carrying capacity of the structure. Furthermore, it may be essential to simulate other structural components of masonry arch bridges, i.e. spandrel walls. This concern arises when poor backing materials and damaged spandrel walls exist. Therefore, advanced three-dimensional numerical models are needed to capture full structural response. The finite element method (FEM) is one of the most popular numerical solutions which forms the foundation of the continuum-based modeling and thus far for masonry arch bridges. The continuum-based macro modelling approach offers practice-oriented option to professionals and engineers with different level of complexity, which can be applied to large scale models in 2D and 3D. However, localized cracks and joint openings may not be represented properly in continuous medium models and for accurate representation of masonry, more detailed micro-modeling solutions are required. In this context, discrete, or discontinuous, approaches have a clear advantage to simulate crack propagations and collapse mechanisms by considering weak mortar joints as a discontinuous displacement field. The main drawback of discontinuous finite element methods is the computational cost and large number of input parameters to characterize masonry as well as the priori knowledge of the discontinuities in the numerical model. Recently, discrete element method is applied on masonry arch structures as an alternative simplified approach to micro-modeling with FEM, by expanding masonry units, while maintaining the discontinuity characteristics at the unit/mortar interface (joints). In DEM models, joints are represented by zero-

thickness interfaces where linear/nonlinear joint constitutive models can be assigned.

Hence, depending on particular concern of the research, the numerical approach may be modified, and necessary simplification can be made without interrupting the overall response of the structure.

## 1.2 Goals and Objectives

In present research, the complete mechanical behavior of masonry arch systems is investigated by means of different numerical modeling strategies. The overarching goal of this dissertation is to better simulate the masonry arch system incorporating discontinuum and continuum based computational modeling strategies. To achieve this goal, it is necessary to take into account following objectives.

### **1) To develop new contact models to be used in discrete element method.**

Commonly used tensile contact constitutive models are not able to represent the complete (pre- and post-peak) response of the material and do not consider the fracture energy in the numerical formulation. As a result of that, newly developed linear and polynomial tensile contact softening models are implemented into a commercial discrete element code, called 3DEC. Next, the proposed contact models including tensile fracture energy are utilized in both detailed and simplified representations of the material. Using this method, the tensile response of unreinforced stack bonded masonry prisms and plain concrete, referred as quasi-brittle construction materials, are studied to capture their pre- and post-peak behavior of these materials via discontinuum type of analysis.

### **2) To compare the different modeling strategies in order to analyze the in-plane capacity of masonry arches.**